QCD at the Large Hadron Collider—Higgs Searches and Some Non-SUSY Extensions Beyond the SM

Prakash Mathews[a] *and V. Ravindran*[b]

[a] *Saha Institute of Nuclear Physics, 1/AF Bidhan Nagar, Kolkata-700064, India*

[b] *Regional Centre for Accelerator-based Particle Physics, Harish-Chandra Research Institute, Chhatnag Road, Jhunsi, Allahabad-211019, India*

We present a brief overview of the physics potential of the Large Hadron Collider LHC and the role of uantum chromodynamics CD in predicting various observables at the LHC with unprecedented accuracy. We have studied the production of Standard Model SM Higgs boson through gluon fusion channel and various signals of physics beyond the Standard Model SM restricted to non-supersymmetric scenarios. These are models with large extra-dimensions such as ADD and Randall-Sundrum models and also physics senario resulting from scale/conformal invariant sector, namely unparticle physics. We have presented CD effects to several of the observables in these models through higher order perturbative CD corrections and parton distribution functions. We have demonstrated how the these corrections reduce the scale ambiguities coming from renormalisation and factorisation. Our study shows that the precise and unambiguous predictions are possible for various SM studies at the LHC.

1. Large Hadron Collider

The Large Hadron Collider (LHC) is a gigantic machine situated at CERN [1], Geneva, spanning the border between Switzerland and France about 100 m underground. This is a particle accelerator specially designed to study the smallest fundamental building blocks that constitute our universe. This is aimed at to shed light on our understanding of the nature at a very fundamental level. It consists of six distinct experiments, characterised by their unique particle detector and the purpose. Out of which, ATLAS and CMS are two large experiments, independently designed for discovery purpose and will serve to study wide range of phenomena at sub atomic level. Two medium-size experiments, ALICE and LHCb are designed to study specific phenomena. The remaining experiments, namely TOTEM and LHCf will focus on forward particles that just brush past each other in the collision region.

At the LHC, two beams of protons will be first accelerated in opposite directions in the underground accelerators of 27 km in circumference, and then collided head-on at close to the speed of light, after they gain very high energy which is around 14 TeV. During the collision, some of the energy will be converted into mass and already known as well as new particles that will unravel the physics which is never explored at the fundamental level. The particles produced due to these collisions will be recorded by specially designed detectors for further study. Since the experiment is going to recreate the environment of our early universe, it will improve our understanding of the basic forces that govern the nature and the mysteries such as the origin of mass, whether there exists extra-dimensions of space not seen so far, evidence for dark matter candidates and microscopic black holes and scale or conformal invariant sectors.

The detectors consist of layers of detector materials to detect and measure the energy or momentum of different particles produced. Particles produced in the collision will pass through the tracking system, made of silicon pixels and silicon strip detectors which record their positions. The momenta of charged particles can be obtained by the curvature of their paths resulting due to the magnets present. The calorimeters in the next layers will record the energies of the particles. They are of two types, the first one records the energies of the electrons and photons called electromagnetic calorimeter (ECAL) and the second one records the those of hadrons (also jets) called hadronic calorimeter (HCAL). Muons that escape these detectors can be detected in the detectors outside these calorimeters from their tracks in the presence of magnets. Neutrons that can not be trapped can be studied from the missing energy and momentum of each collision.

There are several physics issues which the LHC is expected to provide partial or full answers. We discuss here few of them. The most likely explanation of the origin of mass may be found in the Higgs boson predicted by the SM of particle physics [2]. This particle

is yet to be found and the LHC has sufficient energy to discover it. The universe we live is made up of ordinary particles forming only 4%, the rest called dark matter and dark energy forming 96% which are difficult to detect. The supersymmetric particles [3] which may explain the existence of dark matter can be detected at the LHC. The other mystery of our universe is why only tiny fraction of matter survived after Big Bang leaving hardly any antimatter. The LHCb experiment is designed to study the differences between matter and antimatter to find the answer. In the very early universe just after the Big Bang, the temperature would have been very high to overcome the binding strong interaction force between quarks and gluons to form nucleon making new phase of matter called plasma, a very hot and dense mixture of quarks and gluons. The ALICE experiment will recreate conditions similar to those just after the Big Bang to analyse the properties of the quark-gluon plasma. We know that the gravity appears weak as compared to other three interactions of nature. This is called hierarchy problem. Theories with hidden dimensions of space may explain this. String theory implies that there are additional spatial dimensions yet to be observed. Motivated by this idea, models such as large, universal extra-dimensional models [4,5] provide the explanation for the smallness of gravitational interaction. These models may be testable at very high energies and the LHC detectors are also specially designed to look for the signs of extra dimensions. Recently, the idea of detecting a sector which is scale or conformal invariant has been proposed, under the name unparticle physics [6]. This can also be tested at the LHC because these effects can influence various observables significantly.

2. Quantum Chromodynamics

At the LHC the particles that collide are protons which interact through strong interaction force. The theory of strong interaction [7], namely quantum chromodynamics (QCD) plays an important role for all the physics studies to be undertaken at the LHC. QCD describes the dynamics behind the strong force between quarks, anti-quarks and gluons that constitute all the hadrons that we know of.

The theory of strong interaction force is described by the QCD Lagrangian given by

$$\begin{aligned} -_{Q\ \ D} &= -\frac{1}{2}T\ [F^a_{\mu\nu}T^a F^{\mu\nu b}T^b] \\ &\quad + \overline{\psi}[i(\mathbb{I}\partial\!\!\!/ - ig_s A\!\!\!/^a T^a) - m\mathbb{I}]\psi\ . \end{aligned} \tag{1}$$

The above Lagrangian is called the Yang-Mills (YM) Lagrangian. It is invariant under local non-abelian group $SU(3)$. The $SU(3)$ gauge symmetry is called non-abelian gauge symmetry and the gauge fields are called non-abelian gauge fields. The matrix T^a is the generator of the gauge group which in the fundamental representation is a 3×3 matrix. There are 8 such matrices denoted by the index $a = 1,...,8$. The parameters g_s and m are the gauge coupling and quark mass matrix respectively. The fermionic field given by ψ is a three component vector with each component carrying a specific index, called colour index. In other words, each quark or anti-quark comes in three different colour quantum numbers. There are 6 such quarks and 6 anti-quarks, namely up(u), down(d), charm(c), strange(s), top(t), bottom(b) and their charge conjugate partners, called anti-quarks. The kinetic energy part of the $SU(3)$ gauge fields contains second rank tensor fields given by

$$F^a_{\mu\nu} = \partial_\mu A^a_\nu - \partial_\nu A^a_\mu + g_s f^{abc} A^b_\mu A^c_\nu\,. \tag{2}$$

The interaction of gauge fields among themselves comes from $F^a_{\mu\nu}(x)$ in the action Eq. (1) which contains a term $g_s f^{abc}A^b_\mu(x)A^c_\nu(x)$ (Eq. (2)). Notice that the above action describes not only the interaction of 6 quarks (also 6 anti-quarks) with 8 gauge fields, called gluons but also describes the interaction of gauge fields among themselves. This feature is characteristic of theories with non-abelian gauge symmetry. Since the theory of electrons and electromagnetic gauge fields is invariant abelian symmetry i.e. $U(1)$, the electromagnetic gauge fields do not interact with each other. This theory is further quantised and the standard gauge fixing procedure introduces the ghost fields that interact with gauge fields. Hence one has to take into account the ghost field contributions which enter through quantum loops. This theory is also renormalisable. Hence the strong coupling constant g_s that appear in the Eqs. (1, 2) depend on a scale where the theory is renormalised. This scale is called renormalisation scale denoted by μ_R. The standard renormalisation programme can be applied to this theory to find out how the coupling constant changes with the renormalisation scale. One finds that the scale dependence is governed by the renormalisation group equation (RGE), defining

$$a_s = \frac{g_s^2}{16\pi^2}\,, \tag{3}$$

the RGE reads,

$$\mu_R^2\frac{da_s}{d\mu_R^2} = \beta(a_s(\mu_R^2)) = -\sum_{i=0}^{\infty} a_s^{i+2}(\mu_R^2)\beta_i\,, \tag{4}$$

where $\beta(a_s(\mu_R^2))$ is the beta function. The one-loop contribution to it is given by β_0

$$\beta_0 = \frac{11}{3}C_A - \frac{2}{3}n_f T_f\,, \tag{5}$$

where $C_A = 3, T_f = 1/2$. This is positive because $n_f = 6$. The results for β_1, β_2 and β_3 are available in the literature. The solution to Eq. (4) at one-loop level is given by

$$a_s(Q^2) = \frac{a_s(\mu_0^2)}{1 + \beta_0 a_s(\mu_0^2)\ln(Q^2/\mu_0^2)} + \mathcal{O}(a_s^2). \tag{6}$$

Notice that the strong coupling constant decreases as the scale Q increases. It vanishes when $Q \to \infty$. This behaviour is called asymptotic freedom. In other words, the non-abelian theory which describes strong interaction force is a free theory at very high energies. This means that the quarks, anti-quarks and gluons do not interact with other at infinitely high energies. On the contrary, the coupling becomes very large at low energies. Hence at moderately high energies, the coupling constant is not only finite but also a small parameter which can allow us to apply the standard perturbative methods to compute observables involving quark, anti-quarks and gluons. Hence, for the LHC study where the energy scale is large, we can safely apply perturbative methods to compute observables using QCD. Similar renormalisation group analysis for the masses implies that at high energies the masses approach to zero. In addition the energy scales involved at the LHC is so high the effects coming from the finite mass of the quarks except for top quark can be safely ignored.

2.1. QCD Factorisation Theorem

At the LHC, due to large energy available, the high energetic scattering of proton beams will break the protons into their constituents such as quarks, anti-quarks and gluons and the scattering of protons essentially means the scattering of these particles. We call them partons. These partons are so energetic that they can interact and produce the particles we know of through the dynamics summarised by SM of particles. It is capable of producing the Higgs boson which is responsible for symmetry breaking mechanism and for the mass generation of all the particles within the SM. Also we can unravel physics beyond the Standard Model (BSM). That is, the LHC can produce new particles and demonstrate existence of new dynamics which we have not seen in the past. This is possible at the LHC because of the high energy available in each collision but also the high luminosity of the proton beams. These factors will boost the production rates through their large cross sections and luminosity. In addition, the specially designed detectors are capable of recording most important events for the physics study and discovery purposes. Huge statistics and high level detector technologies will make the measurement to an unprecedented accuracy. Hence it is important to have theoretical predictions for various observables at the LHC with least uncertainties so that we will be able not only to test the SM to very good accuracy but also understand any deviations from the SM in terms of phenomena resulting from the physics BSM. The theoretical uncertainties resulting from computations can be estimated and further reduced using the tools developed with aid of various algebraic and numerical techniques. Often the leading order (LO) results are highly sensitive to theory uncertainties. Sometimes, the standard perturbative methods are not suitable for the computation of kinematical distributions in certain phase space regions due large logarithm appearing at every order in perturbative expansion. Analytical computation of the distributions at next to leading order (NLO) involves technical complications which can be solved only by seminumerical approach and it turns out they are most suitable for direct comparison with the experimental results. They are called Monte Carlo approach.

The high energy hadronic cross section involving two protons in the initial state and a specific set of final state particles denoted by X having momenta given by P_X can be written in terms of renormalised partonic cross sections using QCD factorisation theorem [8] as follows:

$$\begin{aligned} d\sigma_{\mathcal{S}}(P_1, P_2, \{P_X\}) &= \sum_{a,b=q,\bar{q},g} \sum_{\{\ \ _I\}} \int_0^1 dx_1 \int_0^1 dx_2 \\ &\times f_{a/\ \ _1}(x_1, \mu_F^2) f_{b/\ \ _2}(x_2, \mu_F^2) \\ &\times \Delta(x_1, x_2, \{P_I\}, \{P_X\}, \mu_F^2) \\ &\times \mathcal{S}(x_1, x_2, \{P_I\}, \{P_X\})\ , \end{aligned} \tag{7}$$

where $f_{a/\ \ }(x, \mu_F^2)$ is the probability of finding a parton of type a inside the proton with a momentum fraction x of the proton. They are called parton distribution functions (PDFs), $\Delta(x_1, x_2, \{P_I\}, \{P_X\})$ is the collinear finite partonic cross section. The incoming partonic states (a, b) with momentum fractions x_1, x_2 and intermediate states (I) with momenta $\{P_I\}$ are summed over. Notice that the massless partons produce divergent cross sections which are mass factorised in a process independent way and then suitably absorbed into bare PDFs leaving the resultant $\Delta(x_1, x_2, \{P_I\}, \{P_X\})$

collinear finite. The scale at which this is done is called factorisation scale, denoted by μ_F. Hence both PDFs and the collinear finite cross sections are individually dependent on μ_F but the observable $d\sigma(P_1, P_2, \{P_X\})$ does not. The function $\mathcal{S}(x_1, x_2, \{P_I\}, \{P_X\})$ take care various constraints that we can impose on the final states. Even though this function uniquely defines the observable we are interested in, it is chosen in such a way that it does not affect the factorisation of collinear singularities.

The PDFs are not computable within perturbative approach because they carry long distance (low energy) part of the cross section. They are usually fitted from the experiment for various values of x and μ_F. The renormalisation group invariance of the hadronic cross section with respect to the factorisation scale controls the scale dependence of the PDFs as well the collinear finite cross sections through perturbatively calculable anomalous dimensions/splitting functions denoted by $P_{ab}(x, \mu_F^2)$

$$\frac{df_{a/\ }(x,\mu_F^2)}{\mu_F^{-2} d\mu_F^2} = \sum_b \int_x^1 \frac{dy}{y} P_{ab}(y,\mu_F^2) f_{b/\ } \left(\frac{x}{y}, \mu_F^2\right). \quad (8)$$

This equation is called DGLAP evolution equation. $P_{ab}(x, \mu_F^2)$ is expanded in powers of a_s

$$P_{ab}\left(x,\mu_F^2\right) = \sum_{=1}^{\infty} a_s(\mu_F^2) P_{ab}^{(\ -1)}(x)\,. \quad (9)$$

The result for P_{ab} upto order a_s^3 is available in the literature [9]. The solution to DGLAP evolution equation determines the scale dependence of these PDFs. One parameterises these initial distributions for the partons at an experimental scale, say Q_{expt} and wide range of x available and then they are compared against the data to fix the parameters of the fit. The fit depends on various factors namely, the range of x and Q_{expt} that the experiments can provide and the accurate theoretical expressions. Fixed target as well as collider experiments such as deep inelastic scattering experiments and proton anti-proton hadronic machines have provided huge amount of rich data to fit these PDFs to a very good accuracy for a wide range of x and Q.

The collinear finite cross sections $\Delta_{ab}(\mu_F^2)$ are computable in perturbative QCD as a series expansion in the strong coupling constant a_s

$$\Delta_{ab}(\mu_F^2) = \sum_{=0}^{\infty} a_s(\mu_R^2) \Delta_{ab}^{(\ )}(\mu_F^2, \mu_R^2)\,, \quad (10)$$

where all the argument except μ_F is suppressed for brevity. The scale μ_R is called the ultraviolet (UV) renormalisation scale at which the theory is renormalised. The computation involves careful treatment of soft and collinear singularities that arise due to soft gluons and massless partons respectively. KLN theorem ensures the cancellation of soft singularities and factorisation theorem, the collinear finiteness. Note that the scales μ_F and μ_R are artifacts of factorisation and renormalisation and hence they should not affect the physical cross sections which are renormalisation group invariants with respect to these scales independently. On the other hand, the truncated perturbative series is not RG invariant. This introduces a scale uncertainty in any fixed order perturbative results. As is clear, the dependence goes down as the order of perturbation increases. The computation of these partonic cross sections beyond LO is feasible only for few process with definite final states due to technical complexities. The results beyond the LO are available only for few processes, for example Drell-Yan, Z, $W^{\pm}$, Higgs, prompt photon, di-photon, di-boson and jet productions, etc. are known to NLO level. In fact, NNLO QCD results for total as well as several kinematical distributions are available only for Drell-Yan, Z, $W^{\pm}$ and Higgs productions. In addition, NLO QCD results resulting from physics BSM are also available for certain processes making the predictions stable under perturbation. The Z and $W^{\pm}$ productions at the LHC at the initial stages of the operation, will be very important to constrain PDF uncertainties in the (x, Q) range not measured by previous experiments. These processes are said to serve as a standard candles. This will help to make unambiguous predictions for other SM processes for precision study as well as for new physics discoveries. A careful analysis indicate that the PDF uncertainties for the rapidity distributions of Z and $W^{\pm}$ at the LHC using the available data from various experiments have reached a precision of around 8% and this is good for using these processes as luminosity monitors. The analytical approach is often not possible if one is interested in the observables involving definite set of final states with well defined kinematic configurations. For example, the choice of the function $\mathcal{S}$ given in Eq. (7) can often make the analytical computation not feasible. The alternate approach is to use numerical approach called parton level generators. Here, one generates parton level events which are weighted with appropriate probabilities given by the partonic scattering matrix elements to predict the cross sections. This way, it is now possible to compute cross sections involving several jets, photons, Z and $W^{\pm}$ etc. Shower Monte Carlo event generators incorporate the hadronisation of final state partons using theoretically motivated models.

Even though these numerical approaches provide theoretical estimates for many realistic observables measurable in the experiments, they are often known at LO level due to technical difficulties involved in implementing higher order matrix elements. NLO improved monte carlo codes for certain observables are already available in the literature for physics study. The fixed order perturbative QCD predictions have limitations in applicability due to the appearance of large logarithms in some kinematical regions of the phase space. In such regions, the applicability of fixed order perturbative results becomes questionable due to the missing higher order corrections that are hard to compute. The alternate approach is to resum these logarithms in a closed form. Such an approach of resuming a class of large logarithms supplemented with fixed order results can almost cover the entire kinematic region of the phase space. In addition, these threshold corrections are further enhanced when the flux of the incoming partons become large in those regions. In the case of Higgs production through gluon fusion, the gluon flux at small partonic energies becomes large improving the role of threshold corrections.

3. Higgs Production Through Gluon Fusion at the LHC

In the SM, the Higgs mechanism is responsible for mass generation and its prediction is existence of the Higgs boson, a neutral scalar particle which couples to fermions and gauge boson. The only unknown parameter here is its mass. In the minimal supersymmetric extension of the standard model (MSSM), one needs two Higgs doublets to preserve supersymmetry and to give mass to the fermions. After symmetry breaking, we are left with two CP even (h, H), one CP odd (A) and two charged higgs $(H^{\pm})$. To lowest order, mass m_A of A and $\tan\beta$, the ratio of vacuum expectation values $v_i, i = 1, 2$ are the unknown parameters. Experiments which are going on for last two decades have set bounds on the mass of the Higgs bosons. The limit coming from the direct searches of SM Higgs boson is 114.4 GeV (at 95% CL) while it is <180 GeV from precision measurements. In the MSSM, at tree level, the lightest neutral Higgs boson has an upper bound of M_Z and it goes up to 130–140 GeV if we include higher order radiative corrections. At the LHC, these Higgs bosons will be produced and the properties can be measured. For example the SM Higgs boson mass can be measured at the per-mille level and its coupling at 5–20% level. If we restrict ourselves to SM Higgs boson and MSSM pseudo scalar A, they are produced largely through gluon-gluon fusion at the parton level through a top quark loop [10]. This LO process is proportional to square of the strong coupling constant $a_s(\mu_R^2)$ and the gluon flux, $\Phi_{gg}(\mu_F^2)$

$$\Phi_{gg}(x,\mu_F^2) = \int_x^1 \frac{dy}{y} f_{g/} \ \ (y,\mu_F^2) f_{g/} \ \ \left(\frac{x}{y},\mu_F^2\right). \quad (11)$$

They bring in un compensated renormalisation and factorisation scale dependencies make the predictions unreliable. The NLO computation [11] that reduces this problem results in large correction by about 80–100% of the LO result making the perturbative predictions questionable. Such a computation involves evaluation of technically complicated two loop integrals with top quarks in the loops and three body phase space integrals. Going beyond NLO is a difficult task and hence a computation at NNLO in the large top quark mass limit has been accomplished to stabilise the perturbative results as well as to reduce the scale uncertainties. Here the top quark degrees of freedom can integrated out which results in an effective Lagrangian containing new tree level interactions of Higgs boson with the gluons as well as photons. The effective Lagrangian for the Higgs boson coupling to gluons reads

$$-_{eff} \ = \ G_H(a_s(\mu_R^2))\phi(x)\mathcal{O}(x)\,, \quad (12)$$

where $\phi(x)$ is Higgs scalar field and $\mathcal{O}(x) = -1/4\ F^a_{\mu\nu}(x)F^{a,\mu\nu}(x)$. The constant G_H is Wilson coefficient which is also function of top quark mass m_t, Fermi constant G_F and the Higgs boson mass m_H. Such an approach is justifiable if the mass of the Higgs boson is in the intermediate mass range, that is of the order of a few hundred GeV. In fact, this approach works very well if the Higgs boson is less than twice of top quark mass. This makes the computation of total cross sections and several distributions at NNLO level possible [12]. At NLO level, this approximation leads to only 1–4% error when the mass of the Higgs boson is less than 220 GeV. The NNLO result computed using the effective theory increases the cross section by about 10–15% and the scale uncertainties go down significantly, which is of the order of 10%. The resummation of soft gluons [13] can be systematically carried out beyond NNLO level. We have used renormalisation group (RG) invariance, collinear (mass) factorisation and Sudakov resummation of QCD amplitudes as guiding principles to perform the resummation in this region. Using the resummed results in $z = m_H^2/\hat{s}$ ($\hat{s}$-parton centre of mass) space we can now predict the soft-plus-virtual parts (also called threshold corrections) of the dominant partonic differential cross sections beyond $\mathrm{N^2LO}$ due to the recent results on three

loop splitting functions [9] and the form factors [14]. The threshold corrections dominate when the partonic scaling variable z approaches its kinematic limit which is 1. They manifest in terms of the distributions $\delta(1-z)$ and $\mathcal{D}_i$, where

$$\mathcal{D}_i = \left[\frac{\ln^i(1-z)}{(1-z)}\right]_+ \qquad i = 0, 1, \cdots \tag{13}$$

The impact of partial soft plus virtual parts of N^3L and N^4L contributions to Higgs production through gluon fusion at the LHC is presented in Fig. 1. The left panel in Fig. 1 shows the total cross for producing Higgs at the LHC against its mass and the right panel contains the dependence on the scale variation. For LO, NLO and NNLO we used the exact results which contain both soft plus virtual as well as regular hard contributions. For N^iL $(i = 3, 4)$, we use only soft plus virtual results extracted from the resummed formula. Here we have set $\mu_F = \mu_R = m_H$. We find that the inclusion of N^iL $(i = 3, 4)$ does not change the cross section much confirming the reliability of the perturbative approach. Defining

$$R^I\left(\mu_R^2\right) = \left(d\sigma^I\left(\mu_R^2 = \ ^2\right)\right)^{-1} d\sigma^I\left(\mu_R^2\right) \tag{14}$$

in the right panel of Fig. 1, we plot R as a function of $\mu/\mu_0 = \mu_R/m_H$, where we have fixed $\mu_F^2 = m_H^2$. It shows that the inclusion of the higher order terms reduces the sensitivity to the choice of the scale. The

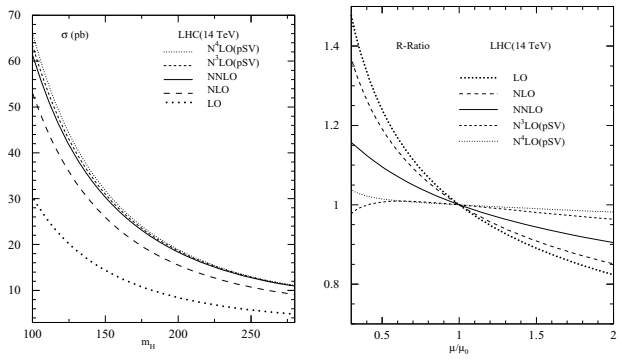

Figure 1. Total cross section for Higgs production through gluon fusion at the LHC, and its scale dependence for the Higgs boson of mass $m_H = 150$ GeV with $\mu = m_R, \mu_0 = \mu_H$. The abbreviation "pSV" means partial soft plus virtual

approach can be systematically extended to to resum the dominant soft gluon contributions to rapidity y distribution of Higgs production [15]. The resummation is done in the $z_i (i = 1, 2)$ space of the kinematic variables, which are the scaling variables that enter the rapidity distribution of the partonic cross sections. The threshold region corresponds to $z_i \to 1$ and in this region all the partonic cross sections are symmetric in $z_1 \leftrightarrow z_2$. Using RG invariance, mass factorisation and Sudakov resummation of QCD amplitudes as guiding principles we have performed the resummation in this region

$$\Delta^{\rm sv}_{gg}(z_1, z_2) = \mathcal{C} \exp\left(\Psi^H_{gg}(z_1, z_2, \varepsilon)\right)\Big|_{\varepsilon=0}, \tag{15}$$

where the symbol $\mathcal{C}$ means that all the normal products resulting from expansion of exponential are replaced by convolutions, sv means soft plus virtual and ε, regulator in the dimensional regularisation. The function Ψ^H_{gg} depends on the gluon form factor F^g, DGLAP kernel Γ_{gg}, the operator renormalisation constant Z_g and the soft distribution function Φ^H_S. Using the above resummed result given in z_i space the predictions are made for the soft-plus-virtual parts of the dominant partonic differential cross sections beyond N^{2}LO. The

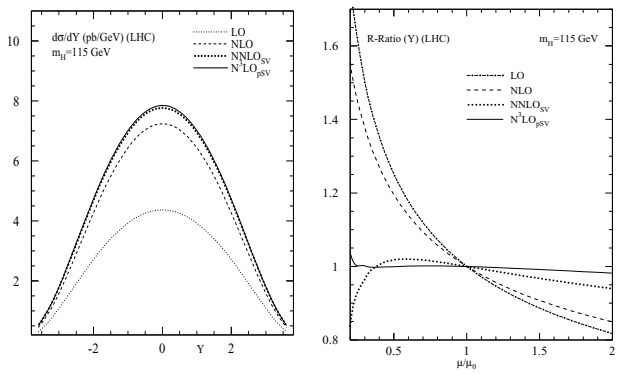

Figure 2. Rapidity distributions for Higgs production through gluon fusion at the LHC, and their μ_R scale dependence for the Higgs boson of mass $m_H = 115$ GeV with $\mu_F = m_H$

impact of soft-plus-virtual parts N^{2}LO and the partial soft-plus-virtual N^{3}LO contributions to Higgs production through gluon fusion at the LHC is presented in left panel of Fig. 2. We see that the inclusion of the higher order terms does not make any appreciable change in

the magnitude of the rapidity distribution. Again this confirms the reliability of the perturbation series. The plot in the right panel of Fig. 2 shows R as a function of $\mu/\mu_0 = \mu_R/m_H$, where again we choose $\mu_F^2 = m_H^2$. We find the inclusion of higher order effect reduces the uncertainty coming from the scale.

4. Non-SUSY Extensions Beyond the SM

The gauge hierarchy problem has been one of the main motivations for physics beyond the SM. The hierarchy between the electroweak scale and the Planck scale is a long standing problem and has been mainly addressed in the past by modifying the particle content of the theory—Supersymmetry (SUSY) and Technicolour belong to this category. A paradigm shift in this approach was proposed by Arkani-Hamed, Dimopoulos and Dvali (ADD) [4] in 1998, wherein they modified the gravity sector instead of additional structure in the particle physics. Though the idea of extra dimension existed since the 1900s, all models assumed that gravity together with all other known interactions could live in the full extra dimensions. Consistency with experimental observations, demands that these extra dimensions be very small. The ADD scenario had explored the possibility of allowing only gravity to probe the extra dimensions and studied the constraints on the size of the extra dimensions. It turns out that for more then one extra dimension, its size could be large without contradicting any known experimental observation and consequently explain the weakness of gravity in 4-dimensions. An alternate solution of the hierarchy problem was suggested by Randall and Sundrum [5] in 1999 with a single extra dimension in a Anti-de-Sitter (AdS_5) metric. The ADD and RS models used the geometry of the extra dimensions to account for the hierarchy between the electroweak scale and the Planck scale.

The idea of extra dimensions has a rich history dating back to 1914 from the initial work of Gunnar Nordström who attempted to unify the electromagnetism and scalar gravity (the only forces then known), by invoking one extra spacial dimension. Later Kaluza (1921) and Klein (1926) tried to unify the electromagnetism and Einstein's general theory of relativity using the same geometrical approach. In the recent times string theory has been the main motivation for extra dimensions as quantised strings are not consistent unless embedded in a ten-dimensional spacetime. In order that these models or scenarios are consistent with present experimental length scale probed at colliders, its essential that these extra dimensions remain hidden. The various extra dimensional models have used different physical mechanism to hide the extra dimensions. The extra dimension could be small and compact, wherein all SM fields are allowed to propagate or alternatively the brane world scenarios wherein the SM particles are confined to the brane and hence can not probe the extra dimensions. In the brane world scenarios the extra dimensions could be of macroscopic size without contradiction with present experiments.

ADD and RS are both brane-world models where gravity exists and only gravity can probe the extra dimensions. Another possibility is the universal extra dimensions (UED) [16] wherein all the SM fields can probe the extra dimension while gravity coupling remains suppressed. Though the UED model has nothing to do with the solution of the hierarchy problem, it could possibly account for dark matter. Various combinations of these scenarios have also been considered. At the LHC it would be possible to test these non-SUSY extensions beyond the SM. In what follows we review some of these non-SUSY extensions beyond the SM and look at its experimental signatures at the LHC. The two main detectors which would be used for this purpose are the general purpose detectors ATLAS and CMS.

4.1. Large Extra Dimensions

In the ADD case the compactified extra dimensions are flat, of equal size and could be large. The large volume of the compactified extra spacial dimension would account for the dilution of gravity in 4-dimensions and hence the hierarchy. This was the first extra dimension model in which the compactified dimensions could be of macroscopic size and consistent with present experiments. In this model, new physics can appear at a mass scale of the order of a TeV. A viable mechanism to hide the extra spacial dimension, is to introduce a 3-brane with negligible tension and localise the SM particles on it. Only the graviton is allowed to propagate the full $4 + d$ dimensional spacetime. As a consequence of these assumptions, it follows from Gauss Law that the effective Planck scale M in 4-dimension is related to the $4 + d$ dimensional fundamental scale M_S through the volume of the compactified extra dimensions [4]. The extra dimensions are compactified on a torus of common circumference R. The number of extra spacial dimension possible is $d \geq 2$ from current experimental limits on deviation from inverse square law [17]. The spacetime is factorisable and the 4-dimensional spectrum consists of the SM confined to 4-dimensions and a tower of Kaluza-Klein (KK) modes of the graviton propagating the full $4 + d$ dimensional spacetime.

The interaction of the KK modes $h^{(\vec{n})}_{\mu\nu}$ with the SM fields localised on the 3-brane is given by

$$-_{int} \sim -\frac{1}{M}\sum_{\vec{n}=0}^{\infty} T^{\mu\nu}(x)\; h^{(\vec{n})}_{\mu\nu}(x)\,, \qquad (16)$$

where $T^{\mu\nu}$ is the energy-momentum tensor of the SM fields on the 3-brane. The zero mode corresponds to the usual 4-dimensional massless graviton. The KK modes are all M suppressed but the high multiplicity could lead to observable effects at the LHC. The Feynman rules are given in [18,19]. The ADD scenario raises the exciting possibility of observing quantum gravity at the LHC.

4.2. Warped Extra Dimensions

In the RS model there is only one extra spacial dimension and the extra dimension is compactified to a circle of circumference $2L$ and further orbifolded by identifying points related by $y \to -y$. Two brane are placed at orbifold fixed points, $y = 0$ with positive tension called the Planck brane and a second brane at $y = L$ with negative tension called the TeV brane. For a special choice of parameters, it turns out that the 5-dimensional Einstein equations have a warped solution for $0 < y < L$ with metric $g_{\mu\nu}(x^\rho, y) = \exp(-2\eta y)\;\eta_{\mu\nu}$, $g_{\mu y} = 0$ and $g_{yy} = 1$. This space is not factorisable and has a constant negative curvature—AdS_5 spacetime. η is the curvature of the AdS_5 spacetime and $\eta_{\mu\nu}$ is the usual 4-dimensional flat Minkowski metric. In this model the mass scales vary with y according to the exponential warp factor. If gravity originates on the brane at $y = 0$, TeV scales can be generated on the brane at $y = L$ for $\eta L \sim 10$. The apparent hierarchy is generated by the exponential warp factor and no additional large hierarchies appear. The size of the extra dimension is of the order of M^{-1}. Further it has been showed that [20] the value of ηL can be stabilised without fine tuning by minimising the potential for the modulus field which describes the relative motion of the two branes. In the RS model graviton and the modulus field can propagate the full 5-dimensional spacetime while the SM is confined to the TeV brane. The 4-dimensional spectrum contains the KK modes, the zero mode is M suppressed while the excited modes are massive and are only TeV suppressed. The mass gap of the KK modes is determined by the difference of the successive zeros of the Bessel function $J_1(x)$ and the scale $m_0 = \eta\; e^{-\pi kL}$. As in the ADD case the phenomenology of the RS model concerns the effect of massive KK modes of the graviton, though the spectrum of the KK mode is quite different.

In the RS model the massive KK modes $h^{(n)}_{\mu\nu}(x)$ interacts with the SM fields

$$-_{int} \sim -\frac{1}{M}T^{\mu\nu}\; h^{(0)}_{\mu\nu} - \frac{e^{\pi kL}}{M}\sum_{n=1}^{\infty} T^{\mu\nu}\; h^{(n)}_{\mu\nu}\,, \qquad (17)$$

where $T^{\mu\nu}$ is the energy-momentum tensor of the SM fields on the 3-brane at $y = L$. The masses of $h^{(n)}_{\mu\nu}$ are given by $M_n = x_n\;\eta\;e^{-\pi kL}$, where x_n are the zeros of the Bessel function $J_1(x)$. In the RS model there are two parameters which are $c_0 = \eta/M$, the effective coupling and M_1 the mass of the first KK mode. Expect for an overall warp factor the Feynman rule of RS is the same as those of the ADD model.

5. Extra Dimension Searches at Hadron Colliders to NLO-QCD

In this section we will consider the brane-world models ADD and RS and study how the KK spectrum would modify the dilepton production at the LHC, which would be produced through the $P_1(p_1) + P_2(p_2) \to \ell^+(l_1) + \ell^-(l_2) + X(P_x)$. The final hadronic state is denoted by X and it carries a momentum P_X. We will also look at how precisely the various observables can be measured subject to the various uncertainties.

At hadron colliders, it is important to have a precise knowledge of the PDFs to predict production cross sections of both signals and backgrounds. These universal PDFs are non-perturbative inputs that are extracted from global fits to available data on DIS, DY and other hadronic processes. Parametrisation of PDFs to a particular order in QCD would involve various theoretical and experimental uncertainties. Recently there has been a series of papers [21–23] which for the first time have calculated the NLO-QCD corrections to various distributions of the DY process for both ADD and RS model. These NLO results would certainly reduce one aspect of the theoretical uncertainties as results prior to this calculation were only to LO in QCD for process involving gravity.

The cross-section $d\sigma/dQ$ as a function of Q to NLO is presented in Fig. 3a for the ADD model [21] and Fig. 4a for RS model [22] at the LHC. We have chosen the representative values of the RS model parameters: $M_1 = 1.5$ TeV the first RS resonance mass and the coupling constant $c_0 = 0.01$. The width of the resonance is related to c_0 and hence a smaller c_0 corresponds to a narrow resonance. The subsequent resonance are determined by m_0 and x_n. To LO the dilepton case has been presented in [24]. To see the effect of the NLO effect we study the K-factor for the Q and Y distribution. The K-factor for the invariant lepton pair mass

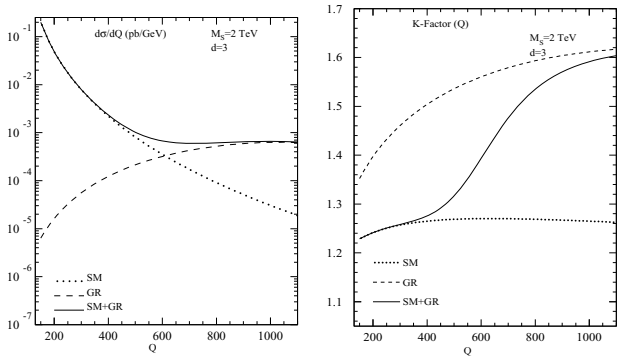

Figure 3. (a) Invariant mass distribution of the dilepton pair production $d\sigma/dQ$ for $M_s = 2$ TeV and $d = 3$ at the LHC to NLO in QCD (left panel). (b) The K-factor for the invariant mass distribution at the LHC (right panel)

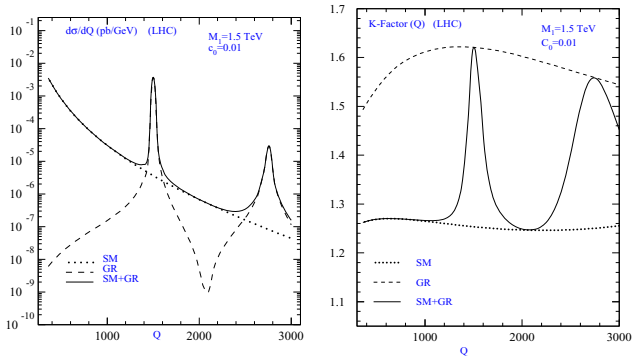

Figure 4. (a) The cross section is plotted as a function of invariant mass Q of the lepton pair for $M_1 = 1.5$ TeV at the LHC (left panel). (b) The corresponding K-factor for Q distribution SM, gravity and SM plus gravity (right panel)

distribution defined by

$$K^I = \left[\frac{d\sigma^I_{LO}(Q)}{dQ}\right]^{-1}\left[\frac{d\sigma^I_{NLO}(Q)}{dQ}\right], \qquad (18)$$

where $I = SM$, $I = SM + GR$ for both SM and gravity combined and $I = GR$ for only gravity. It is possible to define K^{GR} for the invariant lepton pair mass distribution, as there is no interference with SM [21]. The results are presented in Fig. 4b. The parameters chosen are the same as in Fig. 4a.

The spectrum of the KK modes in the ADD and RS models are very distinct. In the ADD case the tower of KK modes leads to an enhancement of the tail of the invariant mass distribution Fig. 3a. In the RS case the KK spectrum consists of a few a few resonance and hence can be seen as resonant enhancement Fig. 4a over the SM.

5.1. Theoretical Uncertainties

In the QCD improved parton model the hadronic cross section can be expressed in terms of the partonic cross section convoluted with appropriate PDF. The subprocess cross section is a perturbative expansion in the strong coupling constant $\alpha_s(\mu_R)$. The partonic flux is non-perturbative and is given in terms of the PDF $f_a(z, \mu_F)$. In perturbative QCD, the unknown higher order corrections and the scale uncertainties are strongly correlated. The factorisation of mass singularities from the perturbatively calculable partonic cross sections leads to the introduction of factorisation scale μ_F in both non-perturbative parton densities $f_a(x, \mu_F)$ as well as the finite partonic cross sections $d\hat{\sigma}_{ab}(x, \mu_F)$. The value of the scale is arbitrary and one demands that the physical cross sections be independent of them. In addition to the factorisation scale, the partonic cross sections are dependent on the renormalisation scale μ_R. This is the scale at which the bare parameters of the theory become finite renormalised ones. The choice of the scale is again arbitrary. Gravity couples to the SM fields via its energy momentum tensor, and the calculations are done in the high energy limits where masses of the SM particles are ignored. Only parameter that requires UV renormalisation is the strong coupling constant. The scale uncertainties come about from the truncation of the perturbative series.

5.2. PDF Uncertainty

Unlike the perturbatively calculable partonic cross sections, the PDFs being non-perturbative in nature are extracted from various experiments. These are fitted at a scale of the experiments and then evolved according to the Altarelli-Parisi evolution equations to any other relevant scale. They are not only sensitive to experimental errors but also to theoretical uncertainties that enter through the partonic cross section calculations and the splitting functions that are known only to certain orders in strong coupling constant in perturbative QCD. There are various groups that are involved in parameterising these PDFs taking the uncertainties into account. These groups use not

only different experiments but also different methods to parametrise these PDFs. Here, we mainly concentrate on the uncertainties coming from the various PDFs, *viz.* Alekhin [25], CTEQ [26] and MRST [27], in detail and quantify their impact on the new physics searches in extra-dimensional models. Differences among the various PDFs would translate as uncertainties on the physical observable. To NLO in QCD for various PDFs, we consider the following differential distributions [28]

$$\frac{d\sigma}{dQ}\,, \qquad \frac{d^2\sigma}{dQ\ dY}\,, \qquad \frac{d^2\sigma}{dQ\ d\cos\theta^*}\,, \tag{19}$$

where Q is the invariant mass, Y the rapidity and the θ^* is the angle between the final state lepton momenta and the initial state hadron momenta in the $c.o.m$ frame of the lepton pair (Figs. 5a, b). The corresponding K-factor which is the ratio of NLO to LO of the above distributions are also plotted for the various PDFs. The K-factor is as large as about 1.6, this clearly shows the need to go beyond LO in QCD in these models [21–23, 28].

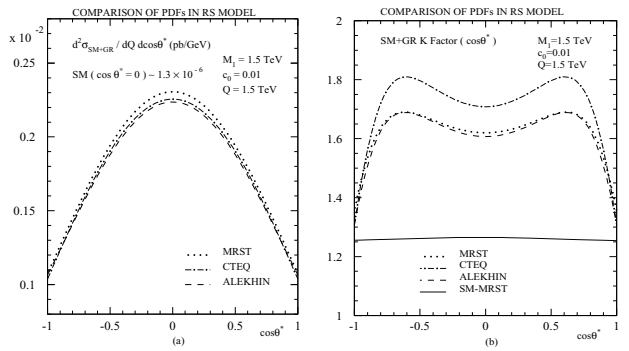

Figure 5. (a) In the region of first RS resonance, the double differential with respect to invariant mass and angular distribution of the lepton is plotted for the various PDFs at the LHC (left panel). (b) The corresponding K-factor for the various PDFs (right panel)

5.3. Renormalisation/Factorisation Scale Uncertainties

The μ_F variation is studied by varying μ_F in the range $0.5\ Q \leq \mu_F \leq 1.5\ Q$. We see that for both the ADD and RS model in going from LO to NLO in QCD, the uncertainties due to μ_F variation considerably get reduced [28]. The spread of K-factor with μ_F is much smaller for the SM as compared to $SM+GR$. This certainly indicates need to go beyond NLO. In Table 1 we tabulate the percentage spread of the factorisation scale μ_F dependence of various distributions at the LHC and Tevatron. On the average at the LHC and Tevatron, the percentage spread of the scale variation get reduced by about 2.88 times in going from LO to NLO. The dependence of cross section on μ_R comes from the strong coupling constant at NLO and at LO there is no μ_R dependence. At NLO μ_R dependence for the Y distribution is plotted for the μ_R range $0.5\ Q \leq \mu_R \leq 1.5\ Q$. The μ_R spread is largest in the central rapidity region and would only reduce at the NNLO level when the μ_R dependences would be compensated for by the dependence coming from the coefficient functions. We have studied the K-factor for SM and $SM+GR$ and see its dependence on μ_R. The uncertainties due to μ_R are much larger when the gravity is included. The percentage spread is of the order of 3.5% which is comparable to the μ_F spread at NLO.

	Distributions	Tevatron		LHC	
		LO	NLO	LO	NLO
ADD	$d^2\sigma/dQdY$	22.8	7.4	9.5	3.5
	$d^2\sigma/dQdcos\theta$	24.2	8.2	10.9	3.8
RS	$d^2\sigma/dQdY$	23.2	7.7	18.7	6.9
	$d^2\sigma/dQdcos\theta$	24.2	8.0	18.4	6.8

Table 1. Percentage spread as a result of factorisation scale variation in the range $0.5Q \leq \mu_F \leq 1.5Q$. For the ADD case $Q = 0.7$ TeV. For the RS first resonance region $Q = 1.5$ TeV for the LHC and $Q = 0.7$ TeV for Tevatron.

5.4. Experimental Uncertainties

In addition to the theoretical uncertainties that we have described in the previous section, there are uncertainties due to errors on the data. Various groups have studied the experimental errors and have estimates of the uncertainties on the PDFs within NLO QCD framework [29,30]. Now that NLO QCD results are also available for extra dimension searches [21] for the dilepton production, we consider some of the distributions and estimate the uncertainties due to the experimental error. We have plotted the error band for the MRST 2001 PDF [30] in the ADD model for the dilepton invariant mass distribution at the LHC. This error band is comparable to the spread associated with the different set

of PDFs [28]. At $Q = 1$ TeV the percentage of experimental error is 7.5% for $SM + GR$ while the pure SM error is about 3.3%. For the RS case at the LHC in the first resonance region at $Q = 1.5$ TeV the experimental error is about 12.8%. At Tevatron the ADD model experimental error is 7.4% at $Q = 1$ TeV. In Fig. 6a we have plotted PDF comparison plots for the double differential distribution with respect to invariant mass and rapidity at a fixed value of $Q = 0.7$ TeV. The experimental error for this distribution for the central rapidity region is about 3.5% and is indicated in the Fig. 6a by the coloured lines.

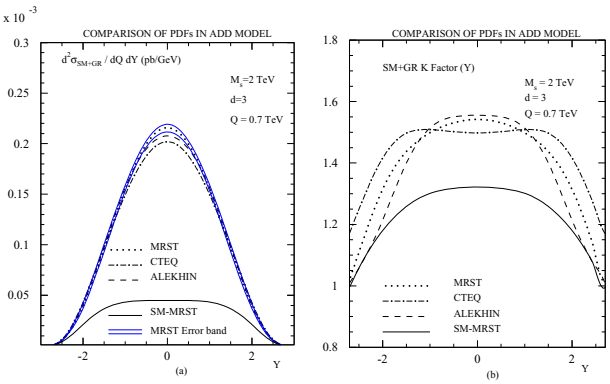

Figure 6. The comparison plots for the various PDFs sets for $Q = 0.7$ TeV at the LHC. (a) The double differential cross section with respect to invariant mass and rapidity as a function of rapidity. The coloured thin line gives the range of experimental error on the MRST PDF (left panel). (b) The corresponding K-factor as a function of rapidity (right panel)

6. Unparticle Physics

In a recent paper, Georgi [6, 31] considered a scenario wherein the SM is weakly coupled to a sector which at an IR scale $\Lambda_{\mathcal{U}}$ has a non-trivial fixed point. At low energies this sector would hence be scale invariant and consequently conventional particle interpretation in this new sector fails—which Georgi termed as unparticle stuff. Essential ingredients of this scenario are (a) the coupling of these unparticle fields to the SM, which makes it possible to look for phenomenological consequences and (b) a mechanism to couple the SM to the unparticle fields which is accomplished by the transition in the Banks-Zaks ($\mathcal{BZ}$) theory [32] from which unparticle physics emerges at low energies.

Banks and Zaks studied the infrared stable fixed point of the $SU_c(3)$ gauge theory with massless fermions. Its well known that the asymptotic freedom of QCD disappears if the number of fermion species n_f or the dimension of their colour representation n_c is too large. QCD β function has been calculated up to 4-loops [33]. It is interesting to study the behaviour of the various coefficients of the β function as a function of n_f for $n_c = 3$. β_3 is positive for all positive values of n_f. As n_f is increased from zero the coefficients of the beta function changes sign as follows: $\beta_2(n_f = 5.844)$, $\beta_1(n_f = 8.05)$ and $\beta_0(n_f = 16.5)$. This indicates the presence of a non-trivial zero of the β function. Now if we denote $n_f = 16.5 = N^*$ and $n_f = 8.05 = N'$ and study the behaviour of β function in the range $N' < n_f < N^*$, we note that as $n_f \to N^*$, the zeros of the β function occurs at lower values of α_s, which implies that the zero of the β function is in the perturbative region. Hence the two loop result is sufficient to extract the IR fixed point. This study of Banks and Zaks showed that for n_f in the range $N' < n_f < N^*$ and close to N^* the theory has an exact scale invariant sector and has no particle interpretation.

Motivated by Banks and Zaks, Georgi [6] proposed the following scheme: Theory at very high energy contains the fields of the SM and fields of a sector called $\mathcal{BZ}$ sector, with a nontrivial IR fixed point. These two sectors interact through exchange of particles with a large mass scale $M_{\mathcal{U}}$. Below $M_{\mathcal{U}}$ the couplings have generic form

$$\frac{1}{M_{\mathcal{U}}^k} \eta_{\rm SM} \eta_{\mathcal{BZ}} \,, \tag{20}$$

where $\eta_{\rm SM}$ and $\eta_{\mathcal{BZ}}$ are operators built out of the SM and the $\mathcal{BZ}$ fields respectively. Scale invariance in the $\mathcal{BZ}$ sector emerges at energy scale $\Lambda_{\mathcal{U}}$. In the effective theory below $\Lambda_{\mathcal{U}}$, the interaction of Eq. (20) matches onto

$$C_{\mathcal{U}} \frac{\Lambda_{\mathcal{U}}^{d_{\mathcal{BZ}} - d_{\mathcal{U}}}}{M_{\mathcal{U}}^k} \eta_{\rm SM} \eta_{\mathcal{U}} \,, \tag{21}$$

where $d_{\mathcal{U}}$ is the scaling dimension of the unparticle operator $\eta_{\mathcal{U}}$ and $C_{\mathcal{U}}$ is a coefficient in the low energy effective theory. $M_{\mathcal{U}}$ should be large enough that its coupling to SM be sufficiently weak. Few of the generic operators that can describe the interaction of unparticle fields with those of the SM are found to be

$$\frac{\lambda_s}{\Lambda_{\mathcal{U}}^{d_{\mathcal{U}}}} T^{\mu}_{\mu}\, \eta_{\mathcal{U}}, \quad \frac{\lambda_v}{\Lambda_{\mathcal{U}}^{d_{\mathcal{U}}-1}} \bar{\psi}\gamma_{\mu}\psi\, \eta^{\mu}_{\mathcal{U}}, \quad \frac{\lambda_t}{\Lambda_{\mathcal{U}}^{d_{\mathcal{U}}}} T_{\mu\nu}\, \eta^{\mu\nu}_{\mathcal{U}} \,. \tag{22}$$

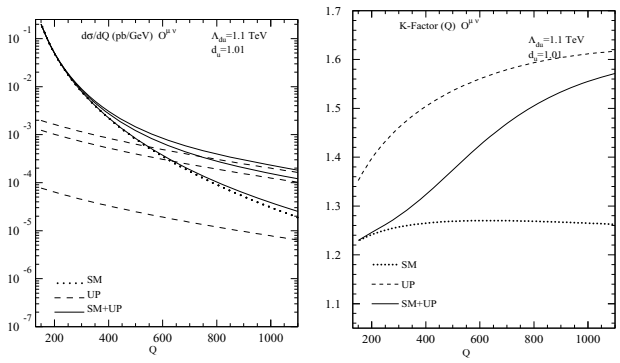

Figure 7. The tensor unparticle coupling to quarks and gluons in the initial state to produce a dilepton pair. (a) Left panel corresponds to the invariant mass distribution of the dilepton Q. The lowest set of lines corresponds to $\lambda_t = 0.4$, middle $\lambda_t = 0.8$ and upper $\lambda_t = 0.9$. (b) Right panel corresponds to the K-factor for the invariant mass distribution

The dimensionless coupling λ_κ corresponds to the unparticle operator $\eta_{\mathcal{U}}^{\kappa}$, where $\kappa = s, v, t$ refers to the scalar, vector and tensor operators respectively. $T_{\mu\nu}$ is the energy momentum tensor of the SM. These operators are Hermitian and transverse.

The unparticle propagator is given by

$$\int d^4x\ e^{i\ \ x}\langle 0|T\eta_{\mathcal{U}}^{\kappa}(x)\eta_{\mathcal{U}}^{\kappa}(0)|0\rangle = \frac{iA_{d_{\mathcal{U}}}}{2\sin(d_{\mathcal{U}}\pi)}\frac{B_\kappa}{(-P^2-i\epsilon)^{2-d_{\mathcal{U}}}}, \tag{23}$$

where B_κ depends on the Lorentz structure of the operator $\eta_{\mathcal{U}}$ as given below

$$\eta_{\mathcal{U}} \qquad 1$$

$$\eta_{\mathcal{U}}^{\rho} \qquad \eta_{\mu\nu}(P) = -g_{\mu\nu} + \frac{\mu\ \ \nu}{\alpha^2}$$

$$\eta_{\mathcal{U}}^{\rho\sigma} \qquad B_{\mu\nu\alpha\beta} = \frac{1}{2}\left(\eta_{\mu\alpha}\eta_{\nu\beta} + \eta_{\mu\beta}\eta_{\nu\alpha} - \frac{2}{3}\eta_{\mu\nu}\eta_{\alpha\beta}\right).$$

The constant $A_{d_{\mathcal{U}}}$ is given by

$$A_{d_{\mathcal{U}}} = \frac{16\pi^{5/2}}{(2\pi)^{2d_{\mathcal{U}}}}\frac{\Gamma(d_{\mathcal{U}}+1/2)}{\Gamma(d_{\mathcal{U}}-1)\Gamma(2d_{\mathcal{U}})}, \tag{24}$$

where $1 < d_{\mathcal{U}} < 2$.

The couplings of the unparticle operators to the SM fields are given by

$$\lambda_\kappa = C_{\mathcal{U}}^{\kappa}\left(\frac{\Lambda_{\mathcal{U}}}{M_{\mathcal{U}}}\right)^{d_{\mathcal{BZ}}}\frac{1}{M_{\mathcal{U}}^{d_{\rm SM}-4}}. \tag{25}$$

A priori we have no information on any of the parameters in the above equation. For our numerical analysis we have taken λ_κ in the range $0.4 \le \lambda_\kappa < 1$, so that the unparticle effects are treated as perturbation. The other parameter that appears in this model is $\Lambda_{\mathcal{U}}$ which we choose to be 1 TeV.

The unparticles could be interpreted as fractional number of massless particles [6] or a collection of particles with a particular mass distribution [34] as a result of deconstruction. It would hence be interesting to look for phenomenological consequences of unparticle phase space or propagator. The coupling of unparticles to the SM Higgs could lead to a constraint on the unparticle sector due to breaking of the scale invariance when the Higgs gets a vacuum expectation value [35]. As a consequence unparticle physics may be relevant at the high energy colliders which have been actively investigated [6, 31, 36–38]. For the dilepton invariant mass distribution we plot the tensor unparticle contribution for various values of λ_t in Fig. 7a and the corresponding K factor in Fig. 7b.

7. Summary

In this article, we have summarised in detail the role of perturbative QCD at the LHC in predicting various SM as well as non-susy observables with least theoretical uncertainties. We have presented a short introduction to the LHC experiment and the basics of perturbative QCD relevant for our theoretical predictions. Higgs boson will be one of the important particles that the LHC will search for. We have studied the impact of NNLO corrections to the Higgs production through gluon fusion in the large top quark mass limit. The results for its total cross section as well as rapidity distribution beyond NNLO are presented using the formalism of soft gluon resummation. The numerical impact these results are presented for a wide range of Higgs masses and rapidities. The results show stability of these observables against higher order perturbation and scale variations. Next we have studied the role played by QCD in predicting various observables resulting from physics BSM such as large extra-dimensional, Randall-Sundrum and unparticle models. The impact of various parton density sets at NLO in QCD on the Drell-Yan production of dileptons at hadron colliders such as the LHC is studied. This process can probe the physics beyond SM through exchange of new particles that these theories predict. At hadron colliders, the precise measurement of DY production cross sections is possible. In this context, we have studied the theories of extra dimensions such as ADD and RS which attempt

to explain gauge hierarchy problem in SM. We have discussed various theoretical uncertainties that enter through renormalisation, factorisation scales and the parton density sets. We have quantified the uncertainties coming from various parton density sets using the recent results on NLO QCD corrections to parton level cross sections and recent PDF sets that take into account various theoretical and experimental errors. Our entire analysis is model independent thanks to the factorisation of QCD radiative corrections from the model dependent contributions. We find that the K-factor for various observable depends on the choice of PDFs.

Acknowledgement: We thank M.C. Kumar and A. Tripathi for discussion. VR thanks J. Smith for discussion. The work of VR has been partially supported by funds made available to the Regional Centre for Accelerator-based Particle Physics (RECAPP) by the Department of Atomic Energy, Govt. of India.

REFERENCES

1. International Europhysics Conference On High Energy Physics fiEPS-HEP2007fi 19-25 Jul 2007, Manchester, England
2. A. Djouadi, Phys. Rept. **457** ff2008fi 1 farfi ivfhep-ph/0503172ffi R. Harlander, J. Phys. G **35** ff2008fi 033001.
3. S. P. Martin, arfi ivfhep-ph/9709356fi A. Djouadi, Phys. Rept. **459** ff2008fi 1 farfi ivfhep-ph/0503173ffi
4. I. Antoniadis, N. Arkani-Hamed, S. Dimopoulos and G. R. Dvali, Phys. Lett. fi **436** fi1998fi 257 farfi ivfhep-ph/9804398ffi
5. L. Randall and R. Sundrum, Phys. Rev. Lett. **83** fi1999fi 3370 farfi ivfhep-ph/9905221ffi W.D. Goldberger and M.fi. Wise, Phys. Rev. Lett. **83** fi1999fi 4922.
6. H. Georgi, Phys. Rev. Lett. **98** ff2007fi 221601 farfi ivfhep-ph/0703260fi
7. T. Muta, Foundations of fi uantum Chromodynamicsfi An Introduction to Perturbative Methods, World Scientific Publishing Company, August 1998.
8. G. Sterman, An Introduction to fi uantum Field Theory, Cambridge fi niversity Press, September 1993.
9. S. Moch, J. A. M. fi ermaseren and A. fi ogt, Nucl. Phys. fi **688** ff2004fi 101 farfi ivfhep-ph/0403192ffi A. fi ogt, S. Moch and J. A. M. fi ermaseren, Nucl. Phys. fi **691** ff2004fi 129 farfi ivfhep-ph/0404111fi
10. F. Wilcfiek, Phys. Rev. Lett. **39**, 1304 fi1977ffi H. M. Georgi, S. L. Glashow, M. E. Machacek and D. fi. Nanopoulos, Phys. Rev. Lett. **40**, 692 fi1978ffi J. R. Ellis, M. fi. Gaillard, D. fi. Nanopoulos and C. T. Sachrajda, Phys. Lett. fi **83**, 339 fi1979fi.
11. S. Dawson, Nucl. Phys. fi **359**, 283 fi1991ffi A. Djouadi, M. Spira and P. M. fi erwas, Phys. Lett. fi **264**, 440 fi1991ffi D. Graudenfi, M. Spira and P. M. fi erwas, Phys. Rev. Lett. **70**, 1372 fi1993ffi M. Spira, A. Djouadi, D. Graudenfi and P. M. fi erwas, Nucl. Phys. fi **453**, 17 fi1995fi farfi ivfhep-ph/9504378fi
12. R. fi. Harlander and W. fi. fi ilgore, Phys. Rev. Lett. **88**, 201801 ff2002fi farfi ivfhep-ph/0201206ffi C. Anastasiou and fi. Melnikov, Nucl. Phys. fi **646**, 220 ff2002fi farfi ivfhep-ph/0207004ffi fi. Ravindran, J. Smith and W. L. van Neerven, Nucl. Phys. fi **665**, 325 ff2003fi farfi ivfhep-ph/0302135fi
13. fi. Ravindran, Nucl. Phys. fi **752**, 173 ff2006fi farfi ivfhep-ph/0603041fi
14. S. Moch, J. A. M. fi ermaseren and A. fi ogt, Phys. Lett. fi **625** ff2005fi 245 farfi ivfhep-ph/0508055fi
15. fi. Ravindran, J. Smith and W. L. van Neerven, Nucl. Phys. fi **767** ff2007fi 100 farfi ivfhep-ph/0608308fi
16. T. Appelfiuist, H. C. Cheng and fi. A. Dobrescu, Phys. Rev. **D64** ff2001fi 035002.
17. C. D. Hoyle *et. al*, *Phys. Rev.* **D70** ff2004fi 042004.
18. G. F. Giudice, R. Rattafiffi and J. D. Wells, *Nucl. Phys.* **B544** fi1999fi 3.
19. T. Han, J. D. Lykken and R-J. fihang, *Phys. Rev.* **D59** fi1999fi 105006.
20. W.D. Goldberger and M.fi. Wise, *Phys. Rev. Lett.* **83** fi1999fi 4922fi *Phys.Lett.* **B475** ff2000fi 275.
21. Prakash Mathews, fi. Ravindran, fi. Sridhar and W.L. van Neerven Nucl. Phys. **B713** ff2005fi 333.
22. Prakash Mathews, fi. Ravindran and fi. Sridhar, JHEP **0510** ff2005fi 031.
23. Prakash Mathews, fi. Ravindran, Nucl. Phys. **B**753 ff2006fi 1.
24. H. Davoudiasl, J.L. Hewett and T.G. Riffio, *Phys. Rev. Lett* **84** ff2000fi 2080fi *ibid. Phys. Rev.* **D63** ff2001fi 075004.
25. S. Alekhin Phys. Rev. D68 ff2003fi 014002.
26. J. Pumplin *et. al.*, JHEP 0207 ff2002fi 012.
27. A.D. Martin *et. al.*, Eur. Phys. J. C23 ff2002fi 73.
28. M. C. fi umar, Prakash Mathews and fi. Ravindran, Eur. Phys. J. C49 ff2007fi 599.
29. S. I. Alekhin, Phys. Rev. D 63 ff2001fi 094022fi CTEfi Collaborationfi J. Pumplin et al., JHEP 0207 ff2002fi 012.
30. A.D. Martin *et. al.*, Eur. Phys. J. C28 ff2003fi 455.
31. H. Georgi, Phys. Lett. fi **650** ff2007fi 275.
32. T. fi anks and A. fi aks, Nucl. Phys. fi **196**, fi1982fi 189.
33. T. van Ritbergen, J. A. M. fi ermaseren, S. A. Larin Phys. Lett. fi 400 fi1997fi 379.
34. M. A. Stephanov, Phys. Rev. D **76** ff2007fi 035008.
35. P. J. Fox *et al.*, Phys. Rev. D **76** ff2007fi 075004fi A. Delgado *et al.*, JHEP **0710** ff2007fi 094fi M. fi ander *et al.*, Phys. Rev. D **76** ff2007fi 115002.
36. fi. Cheung, W. fi. fi eung and T. C. fi uan, Phys. Rev. Lett. **99** ff2007fi 051803.
37. P. Mathews and fi. Ravindran, Phys. Lett. fi **657** ff2007fi 198.
38. M. C. fi umar *et al.*, Phys. Rev. D **77** ff2008fi 055013.